Hindawi
Geofluids
Volume 2022, Article ID 7809560, 16 pages
https://doi.org/10.1155/2022/7809560

Research Article

Investigation on Coal Pillar Stability between Different Shapes of Gasifier Cavities under High Temperatures during UCG

Yue Shi,[1] Xiaopeng Yun,[1] Jianping Zuo,[1,2] Zhengdai Li,[1] Yunjiang Sun,[1] and Meilu Yu[1]

[1]*School of Mechanics and Civil Engineering, China University of Mining and Technology (Beijing), Beijing 100083, China*
[2]*State Key Laboratory of Coal Resources and Safe Mining, China University of Mining and Technology (Beijing), Beijing 100083, China*

Correspondence should be addressed to Xiaopeng Yun; yxp19820000@163.com and Jianping Zuo; zjp@cumtb.edu.cn

Received 19 October 2021; Accepted 15 January 2022; Published 16 February 2022

Academic Editor: Dan Ma

The shape of the gasifier cavity and the high temperatures induced by underground coal gasification (UCG) have a significant influence on the failure characteristics of the surrounding rock. In this study, the variations in the mechanical properties of the surrounding rock in gasifier cavities subjected to different temperatures (20–700°C) were obtained experimentally, and the results were used to establish numerical models. FLAC^{3D} was used to analyse the failure of the surrounding rock in drop-shaped and traditional rectangular gasifier cavities. The mechanical parameters of the surrounding rock in the numerical model were assigned a gradient distribution based on the temperature propagation law and the experimental results. The results revealed that the temperature of the surrounding rock has a significant influence on the coal pillar stability, and the surrounding rock primarily undergoes shear failure. As the temperature of the surrounding rock increases, the width of the stable coal pillar increases exponentially; the reasonable widths for coal pillars between adjacent drop-shaped gasifier cavities are 12 m (room temperature), 17 m (700°C and 850°C), 18 m (1000°C), 19 m (1150°C), and 20 m (1300°C). In contrast, the reasonable width of coal pillars in traditional rectangular gasifier cavities is approximately 21 m, which is significantly higher than that for drop-shaped gasifier cavities.

1. Introduction

Underground coal gasification mining is a safe, efficient, and green mining technology, and offers better safety, environmental protection, and adaptability than traditional mining methods [1–4]. During underground coal gasification, as the gasifier cavities expand, the suspended roof area expands continuously, resulting in the movement and breaking of the overlying strata. In addition, the physical and mechanical properties of the surrounding rock of the gasifier cavities are altered by the high temperature, and the characteristics of the resulting deformation and failure of the surrounding rock are fundamentally different from those of traditional mining processes. These characteristics have a significant effect on the reasonable width of the coal pillars between two gasifier cavities. Therefore, the failure characteristics of the surrounding rock in coal gasifier cavities must be studied, and a method to determine the reasonable coal pillar width between adjacent gasifier cavities with different temperatures and shapes must be developed.

Numerous scholars have studied the stress field and failure mechanism of the surrounding rock in underground coal gasifier cavities. Mehdi [5] studied the stress field, fissure evolution, fracture regularity, and stability of coal pillars in the overlying strata of gasifier cavities using FLAC^{3D}. Wang et al. [6] established an equation to calculate the one-dimensional heat conduction of temperature fields in the top and bottom plates of gasified coal seams. They revealed that the temperature of the surrounding rock and coal seam first increases and then decreases. Huang et al. numerically investigated the evolution law of the temperature field, stress field, and displacement field of the surrounding rock in the goaf area during strip mining, considering the thermal–mechanical coupling of

underground gasification using COMSOL [7]. The stress and deformation characteristics of surrounding rock after gasification and conventional mining processes were compared and analysed as well. Based on the theory of thermodynamics and elastic mechanics, Lu et al. [8] developed a temperature–stress coupling control equation considering the evolution of rock failure; the evolution law of the temperature field and fracture field of the overlying rock in the goaf under temperature–stress coupling was numerically analysed as well. Tan [9] used finite element software to simulate the temperature and stress fields of layered rocks at the top and bottom of the coal seam in an underground coal gasification project under linear elastic and nonlinear conditions, considering that the rock specific heat, thermal conductivity, and linear expansion coefficient vary with temperature. Derbin [10] summarised the correlation between different coal seam parameters, gasification-related parameters, and surface subsidence. Sattesh [11] analysed the expansion law of lignite gasifier cavities during underground coal gasification through laboratory tests. Based on data of an underground coal gasification experimental area, Laouafa [12] summarised the influence of underground coal gasification on the surrounding environment and surface subsidence. Considering the observation station of overburden movement and the surface subsidence of a strip underground gasification face, Xin [13] analysed the surface movement and deformation due to insufficient mining. Through numerical simulations, Li [14] investigated the influence of different factors (arch height, pillar height, pillar width, and mechanical characteristics) on the ultimate bearing capacity of hyperbolic pillars at high temperatures and proposed a stability evaluation method. Moreover, innovation and stability analysis of coal columns have been studied by some scholars [15–23] Although studies have primarily focused on the impacts of high temperatures on the surrounding rock in underground coal gasifier cavities, most of the studies only considered traditional rectangular gasifier cavities; consequently, the surrounding rock failure and reasonable coal pillar width of drop-shaped gasifier cavities have not been sufficiently analysed.

Herein, the physical and mechanical properties of the surrounding rock in a coal gasification project in a coalfield in western China are experimentally studied at different temperatures (20–700°C). The experimental results are incorporated into a numerical model that addresses the stress field, displacement field, and failure characteristics of the surrounding rock in traditional rectangular and drop-shaped gasifier cavities at room temperature. The differences in the failure characteristics of the surrounding rock with different coal pillar widths are analysed at different temperatures, and a reasonable coal pillar width is determined. The results of this study can provide guidance on the scientific exploitation of underground coal gasification.

2. Engineering Background

The average depth and thickness of the gasified coal seams in the project are 650 m and 10 m, respectively. The CRIP gasification process is adopted herein. The gasifier cavities are genuine drop-shaped gasifier cavities. The temperature range of the surrounding rock around the gasifier cavities is 1000–20°C (room temperature) during gasification. A coal pillar is set between adjacent gasifier cavities.

The gasifier cavities of underground coal gasification are drop-shaped [24], as shown in Figure 1. The height of the gasifier cavity is longer than its width, and the height-to-width ratio of the gasifier cavity is the highest at the axis of the cavity; the bottom of the gasifier cavity is bowl-shaped. Based on the coal seam thickness and drop-shaped gasifier cavities, a numerical model was built using FLAC^{3D}, as shown in Figure 2. The overall dimensions of the model are $14\,m \times 7.8\,m \times 10.5$ m.

3. Experiments on Physical and Mechanical Properties of Rocks at Different Temperatures

3.1. Experimental Equipment and Experimental Scheme. As shown in Figure 3, experimental tests on the rock mechanics were performed using the GCTS RTR-1000 rock triaxial test system [25,26] in the State Key Laboratory of Coal Resources and Safe Mining, China University of Mining and Technology (Beijing). Various mechanical parameters such as the elastic modulus, Poisson's ratio, and tensile strength of the rock were obtained through uniaxial compression and Brazilian splitting tests.

The rock samples examined were obtained from a coal gasification project in a coalfield in western China. The rock was processed into 25 ∗ 50 mm and 50 ∗ 100 mm test specimens. From all processed test specimens, some test specimens of each type rock with good appearance, close weight, and close porosity were selected for experiments (Figure 4).

The Brazilian splitting test was performed at room temperature, whereas the uniaxial compression tests were performed at different temperatures. A total of nine specimens were subjected to the Brazilian splitting test. The specimens were tested by applying displacement control (5 mm/min) until rupture. A total of 21 specimens were subjected to uniaxial compression tests. The rock specimens [27] were slowly heated to temperatures of 100–700°C in a muffle furnace and maintained at the desired temperature for 3 h. Subsequently, the specimens were naturally cooled to room temperature. Uniaxial compression was performed through strain-controlled loading at a rate of 0.05%/min, until the rock specimen failed.

3.2. Analysis of Test Results of Mechanical Parameters of Surrounding Rock. The tensile strength, elastic modulus, peak strength, Poisson's ratio, and other experimental mechanical parameters of the rock were obtained from the Brazilian splitting test and uniaxial compression tests performed at different temperatures. The curves of the relative density, relative elastic modulus, relative Poisson's ratio, and relative tensile strength ratio with the variation in temperature were obtained by dividing the values of the physical parameters at elevated temperatures by those at room

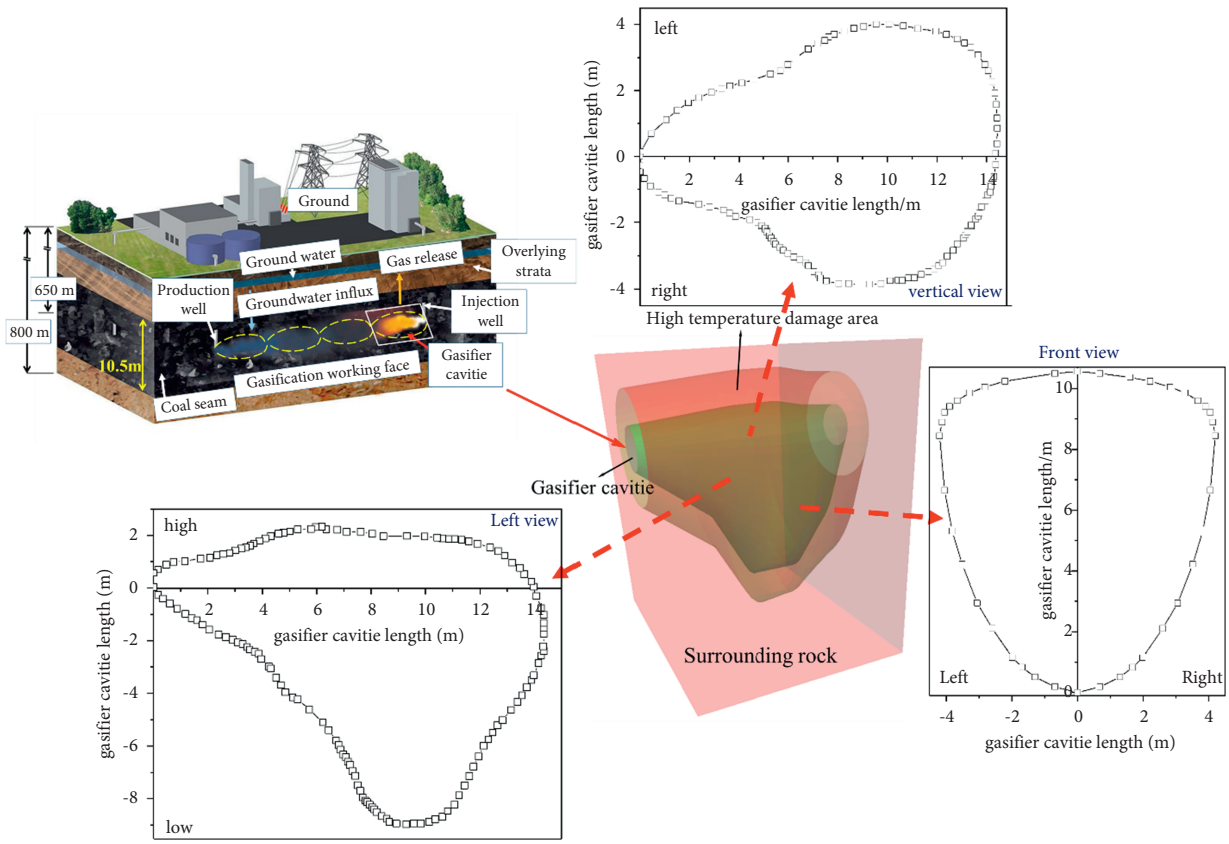

Figure 1: Modelling of drop-shaped gasifier cavities.

Rock formation name	Thickness (m)	Lithological column	Lithology description
Fine sandstone	6.1		Light grayish green, argillaceous cementation, fine grain structure.
Siltstone	11.2		Light grayish green, argillaceous cementation, powder grain structure.
Mudstone	37.7		Grey-black, massive, uneven fracture, relatively broken core.
coal	10.5		Black, lumpy, stepped fracture, dim luster, mainly dark coal.
Siltstone	15.4		Light grayish green, argillaceous cementation, powder grain structure.
Sandy mudstone	8.35		Black, lumpy, uneven fracture, with a lot of carbon chips.
Fine sandstone	7		Light grayish green, argillaceous cementation, fine grain structure.

Figure 2: Histogram of coal seam and strata of - 650 m level.

temperature (Figure 5). As the temperature increased, the physical parameters of the rock weakened. This weakening process can be divided into two stages: one between 20°C and 300°C, when the degree of the high temperature attenuation of the physical parameters of the rock increased rapidly, and the other between 300°C and 700°C, when the degree of the high temperature attenuation of the physical parameters of the rock gradually decreased. At the same temperature, the high temperature attenuation degree of different rocks shows the following order siltstone < mudstone < sandy mudstone. Therefore, sandy mudstone is more sensitive to temperature than mudstone and siltstone. By fitting the

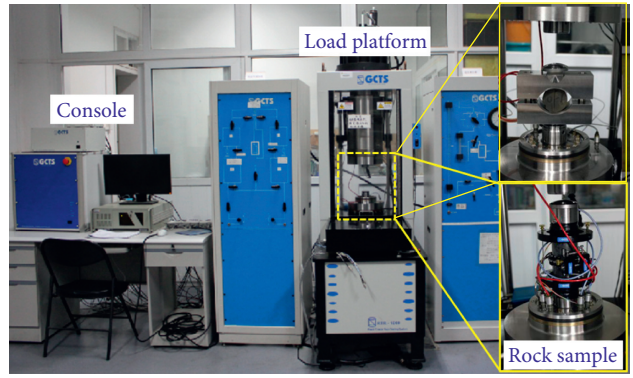

Figure 3: Schematic diagram of GCTS petrophysical laboratory and uniaxial compression/Brazilian splitting tests.

(a) (b)

Figure 4: Uniaxial compression/Brazilian splitting test specimens. (a) 50 ∗ 100 mm uniaxial compression test specimens (b) 25 ∗ 50 mm Brazilian splitting test specimens.

normalised parameters of the rock samples with temperature, the reduction in the relative density with the increase in temperature can be expressed as a linear equation, the reduction in the relative elastic modulus with the increase in temperature can be expressed as a power function equation, the reduction in the relative Poisson's ratio with the increase in temperature can be expressed as an exponential equation, and the reduction in the relative tensile strength with the increase in temperature can be expressed as a linear equation. Notably, the fitting accuracy is good. The temperature sensitivity of the elastic modulus is high, and its attenuation at high temperatures is the highest. The fitting equations can be used as the empirical formulae of the attenuation of the rock physical parameters with the increase in temperature, and form the basis of the high-temperature weakening of the physical parameters of the surrounding rock of the gasifier cavities in the numerical simulation.

4. Numerical Model Establishment and Numerical Simulation

4.1. Numerical Modelling of Gasifier Cavities. Considering the characteristics a coal seam, a traditional rectangular gasifier cavity with dimensions of $14\,m \times 7.8\,m \times 10.5$ m was established herein. The dimensions of the numerical simulation model were $56\,m \times 40\,m \times 160$ m. It comprises two adjacent traditional rectangular gasifier cavities in the middle of the model coal seam, with real and complete surrounding rock outside the gasifier cavities. The overall model had 105,393 nodes and 96,768 elements, with a minimum element size of $1\,m \times 1\,m \times 0.5$ m, as shown in Figure 6(a) and 6(b). The size and position of the drop-shaped gasifier cavities were the same as those of the traditional rectangular gasifier cavities. The entire model contained 251,507 nodes and 243,712 elements. The minimum element size was $0.5\,m \times 0.5\,m \times 0.25$ m, as shown in Figure 6(c) and 6(d). To simulate the weakening effect of high temperatures on the physical parameters of the rock, the surrounding rock in a certain area around the gasifier cavities was weakened using the temperature distribution function, based on the drop-shaped gasifier cavities at room temperature.

A lateral horizontal displacement constraint and bottom vertical displacement constraint were set as the boundary conditions in the numerical model. The depth of the model was 650 m, with a vertical stress of 16.25 MPa applied at the top of the model. The lateral pressure coefficient was set to 1, and the influence of the tectonic stress and boundary effect were ignored. The Mohr–Coulomb

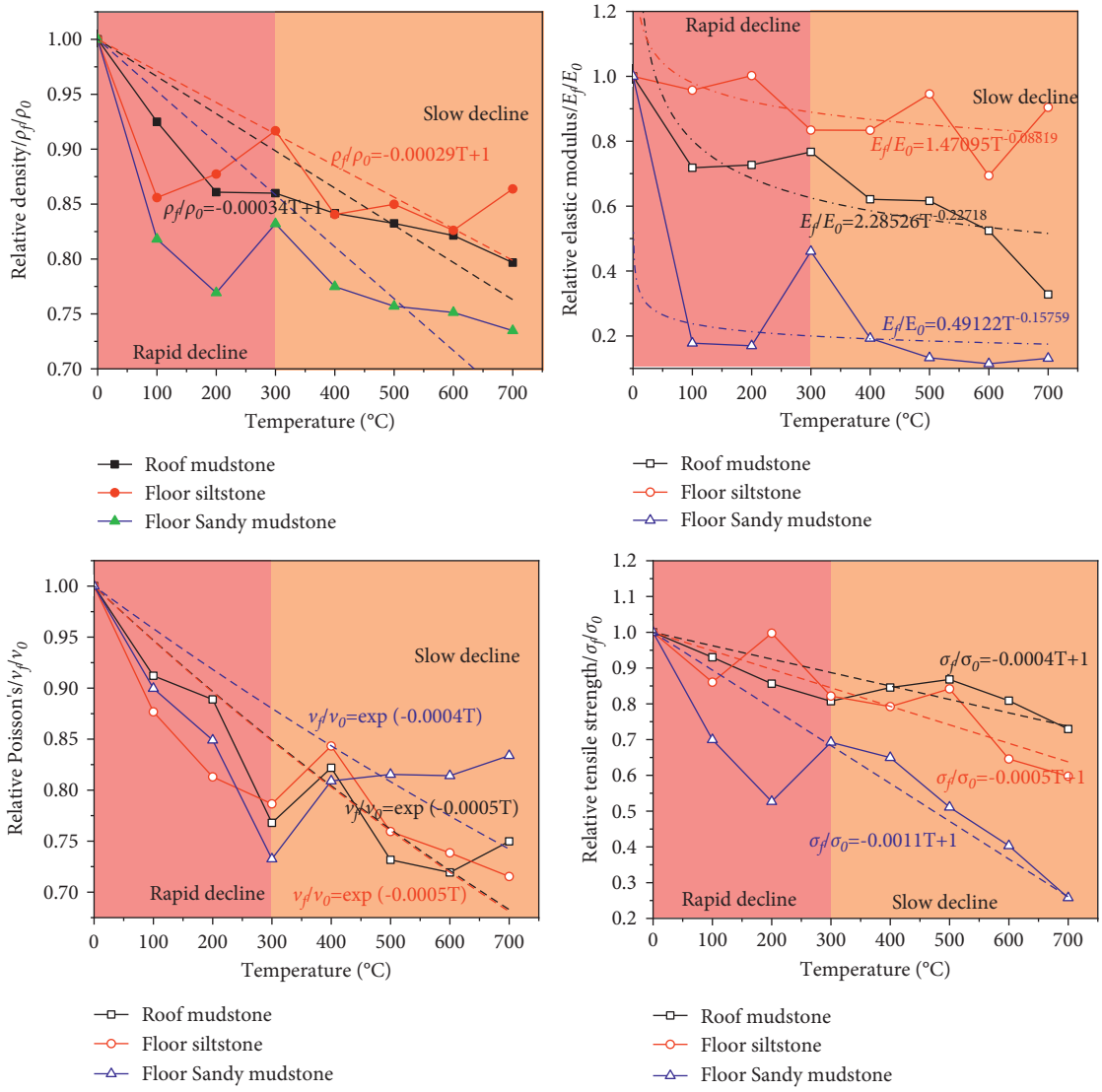

Figure 5: Uniaxial compression test and Brazilian test curve fitting.

failure criterion was used in the model. Plastic flow and dilatancy were not considered in the calculations. The physical and mechanical parameters of the coal and the rock mass are shown in Table 1.

4.2. Failure Weakening Range of Surrounding Rock at High Temperatures. The mechanical tests demonstrated that as the temperature increases, rock exhibits different degrees of failure, and the physical parameters of the rock weaken correspondingly. The effects of the high temperatures induced during coal gasification in the surrounding rock around the coal seam extend to approximately 20 m [24] (Figure 7). The histogram of the coal seam and strata (Figure 2) indicates that the temperature range of failure in the simulation of underground coal gasification is related to the failure of roof mudstone, floor siltstone, and floor sandy mudstone.

The temperature distribution in the gasifier cavities and its top and bottom plates satisfies a linear function [28–30]:

$$T_x = \frac{(T_1 - T_2)x}{l} + T_2,$$
$$T_2 = \frac{(w - l)}{w}, \quad (1)$$

where T_1 is the gasifier temperature of the coal wall in front of the gasifier cavity, °C; T_2 is the surface temperature of the top and bottom of the coal wall in the rear of the gasifier cavity, 20°C; T_x is the surface temperature of the top and bottom of the coal wall in the rear of the gasifier cavity, °C; l is the length of the coal bed, m; and w is the estimated gasifier length of the coal seam, m.

4.3. Numerical Simulation Scheme. Numerical simulations were performed considering different widths of the coal columns between two adjacent gasifier chambers with different shapes at different temperatures. The simulation scheme is shown in Table 2.

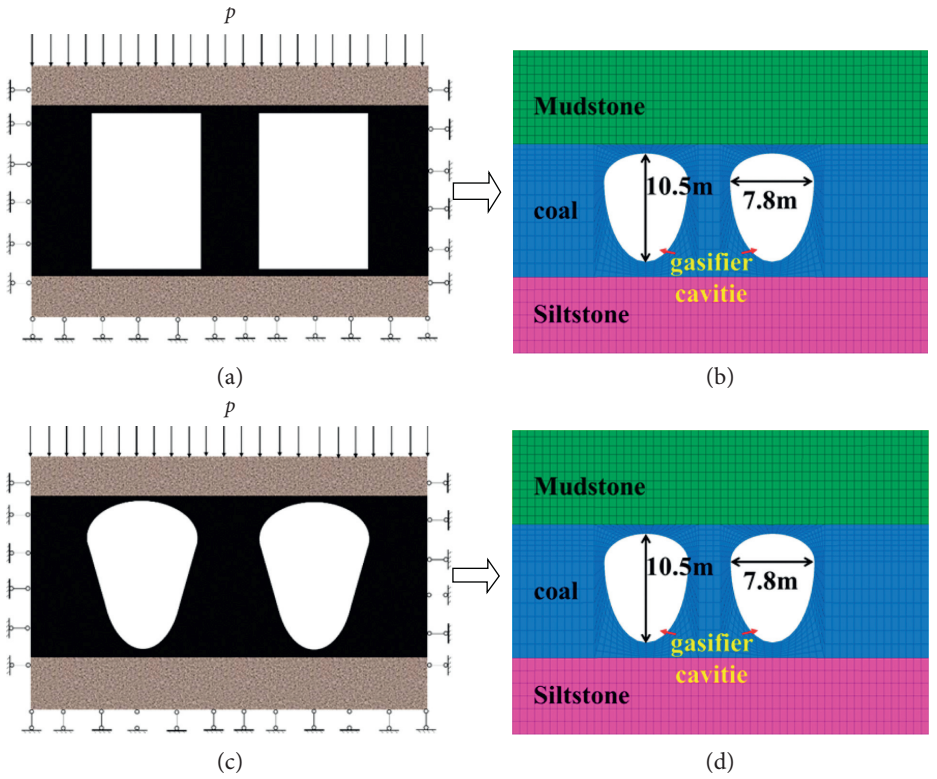

Figure 6: Numerical analysis model of surrounding rock stability of in gasifier cavities: (a) force analysis diagram of the traditional rectangular gasifier cavities; (b) numerical model diagram of the traditional rectangular gasifier cavities; (c) force analysis diagram of the drop-shaped gasifier cavities; and (d) numerical model diagram of the drop-shaped gasifier cavities.

Table 1: Mechanical parameters of strata.

Rock	ρ(Kg/m^3)	K(GPa)	G(GPa)	c(MPa)	σ_t(MPa)	φ(°)
Coal	1421	2.67	1.32	1.20	0.85	20.40
Mudstone	21.47	10.2	5.23	1.30	1.16	23.20
Siltstone	22.05	9.31	5.32	1.60	1.11	38.60
Sandstone	23.11	8.33	5.24	1.50	1.85	36.60
Sandy mudstone	23.16	5.56	2.42	1.40	1.60	28.20

[1] ρ: density; K: bulk modulus; G: shear modulus; c: cohesion; σ_t: tensile strength; φ: internal friction angle.

5. Influence of Different Gasifier Cavity Shapes on the Surrounding Rock at Room Temperature

5.1. Comparison of Plastic Failure Areas and Analysis of Reasonable Coal Pillar Width. The distribution of the plastic failure areas of the surrounding rock in adjacent gasifier cavities of two different shapes, with different coal pillar widths, at room temperature was obtained through simulations. The plastic areas of the surrounding rock initially fuse together, and then gradually detach from each other as the width of the coal pillar increases. The distribution of the plastic failure areas of adjacent traditional rectangular gasifier cavities is shown in Figure 8(a). When the width of the coal pillar is less than 21 m, all the coal pillars undergo plastic failure, and when the width of coal pillar exceeds

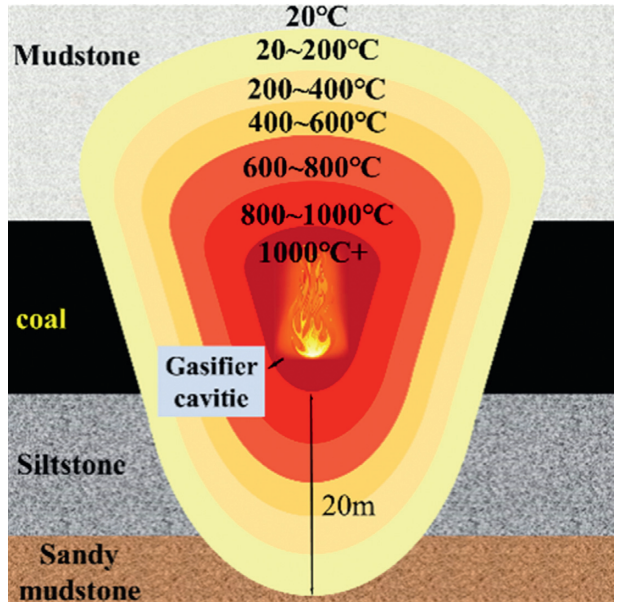

Figure 7: Gasification area of influence.

21 m, a stable elastic area appears in the middle of the coal pillar. As shown in Figure 9(a), the plastic failure of the surrounding rock is primarily shear failure, which is accompanied by a small amount of tensile failure. The volume of rock experiencing shear failure increases with the increase in the width of the coal pillar; it gradually becomes constant

Table 2: Simulation scheme.

Temperature		Gasifier cavities shape	Coal pillar width
Room temperature (20 ˚C)		Traditional rectangular	6m–25 m 6m–25 m
High temperature	700 ˚C 850 ˚C 1000 ˚C 1150 ˚C 1300 ˚C	Drop-shaped	15m–21 m

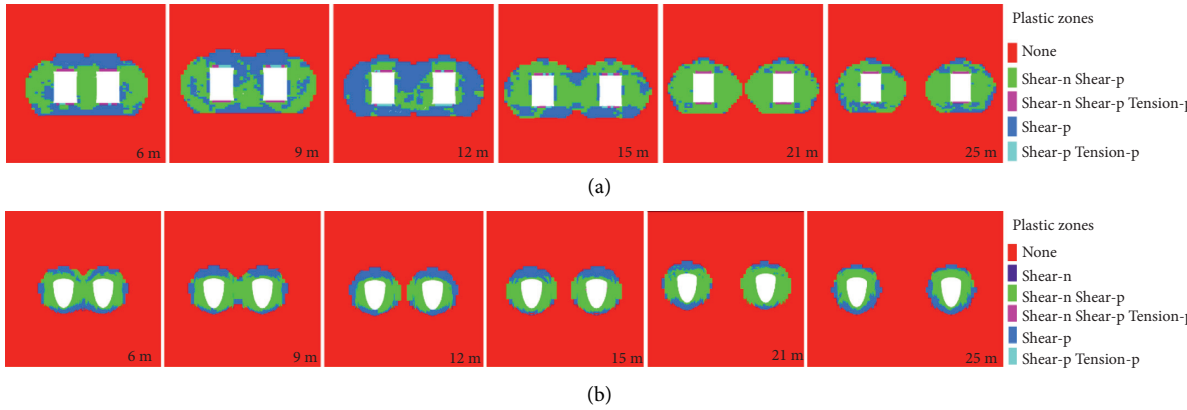

Figure 8: Plastic failure areas of surrounding rock in gasifier cavities with different shapes and pillar widths at room temperature: (a) traditional rectangular gasifier cavities and (b) drop-shaped gasifier cavities.

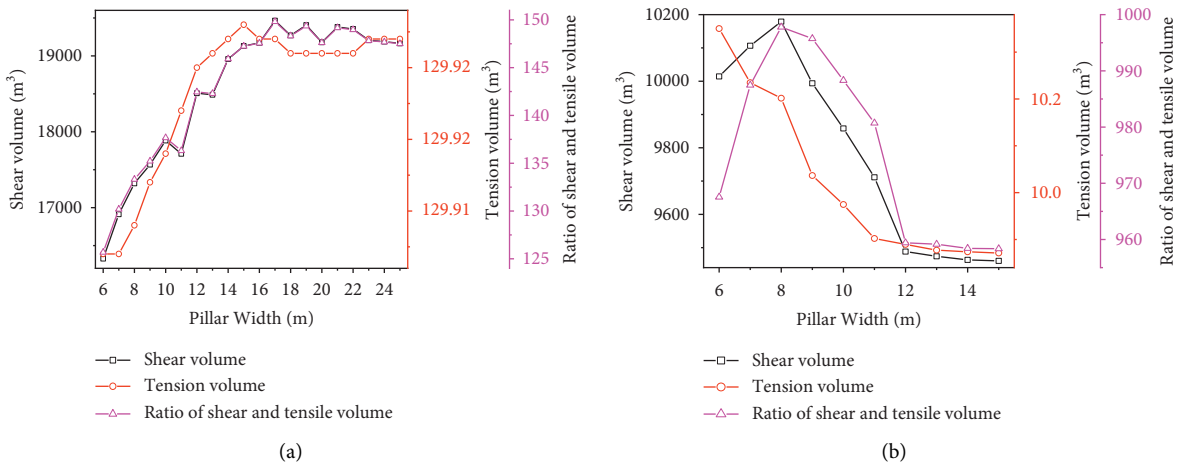

Figure 9: Volume change curves of different plastic failure methods for different gasifier cavity shapes and coal pillar widths at room temperature: (a) traditional rectangular gasifier cavities and (b) drop-shaped gasifier cavities.

and reaches the maximum value when the width of the coal pillar is approximately 17 m. The volume of rock experiencing tensile failure also increases with the increases in the width of the coal pillar; it reaches the maximum value when the width of coal pillar is approximately 15 m, and then gradually decreases. The ratio of the volume of the shear unit to that of the tensile unit is the same as the volume of the shear failure unit. The ratio of the shear unit volume to the tensile unit volume is consistent with the variation trend and reaches the maximum value when the width of the coal pillar is approximately 17 m. Therefore, under room temperature conditions, the reasonable coal pillar width between two adjacent traditional rectangular gasifier cavities should not be less than 21 m.

The distribution of the plastic failure areas of adjacent drop-shaped gasifier cavities is shown in Figure 8(b). When the width of the coal pillar is less than 11 m, all the coal pillars exhibit plastic failure. When the width of the coal pillar exceeds 11 m, a stable elastic area appears in the middle of the coal pillar. As shown in Figure 9(b), the plastic failure in the surrounding rock primarily occurs as shear failure, and tensile failure is almost non-existent. The volume of the

shear failure unit initially increases with the increase in the width of the coal pillar, and then decreases rapidly and tends to remain constant. The volume of the shear failure unit is maximum when the width of the coal pillar is approximately 8 m, and tends to remain constant when the width of the coal pillar is approximately 12 m. The volume of the tensile failure unit initially decreases rapidly with the increase in the width of the coal pillar and eventually tends to remain constant. When the width of the coal pillar is approximately 12 m, the reduction rate decreases significantly. The ratio of the shear unit volume to the tensile unit volume increases with the increase in the coal pillar width, and the ratio is maximum when the width of the coal pillar is approximately 8 m. Furthermore, the reduction rate decreases when the width of the coal pillar is approximately 12 m. Therefore, at room temperature, the reasonable coal pillar width between two adjacent drop-shaped gasifier cavities should not be less than 12 m.

Comparing the plastic failure areas in gasifier cavities with different shapes at room temperature, it can be inferred that the range of the plastic failure areas in the surrounding rock of traditional rectangular gasifier cavities is larger than that of in the surrounding rock in drop-shaped gasifier cavities. Furthermore, the plastic failure areas of traditional rectangular gasifier cavities are dominated by shear failure and direct top/bottom tensile failure, whereas those of drop-shaped gasifier cavities are dominated by shear failure, and tensile failure is almost negligible.

5.2. Comparative Analysis of Stress and Displacement Fields. The stress field distribution of the surrounding rock in two adjacent gasifier cavities with different shapes and coal pillar widths at room temperature was obtained through simulations. The superposition of the stress fields of the two gasifier cavities was observed; the peak stress field was located in the middle coal pillar position, and the peak stress gradually decreased as the coal pillar width increased. The distribution of the stress field in the surrounding rock of the traditional rectangular gasifier cavities is shown in Figure 10(a). The top/bottom plates of the gasifier cavities are in a tensile stress state, and the peak stress of the surrounding rock occurs at the position of the coal pillar. A certain stress concentration area also exists on both sides of the gasifier cavities. The maximum stress of the direct top area initially decreases and then increases with the increase in the coal pillar width; it reaches the minimum value when the coal pillar width is approximately 18–21 m. The maximum stress of the coal pillar initially increases and then slowly decreases, reaching the maximum value when the coal pillar width is approximately 18–19 m. The maximum vertical stress at the roof of the traditional rectangular gasifier cavities and the maximum vertical stress variation curve of the coal pillar for different coal pillar widths are shown in Figure 10(b). The distribution of the stress field in the surrounding rock of the drop-shaped gasifier cavities is shown in Figure 10(c). The stress field of the drop-shaped gasifier cavities is different from that of the traditional rectangular gasifier cavities. The direct top/bottom areas of the drop-shaped gasifier cavities are in a compressive stress state, and the peak stress of the surrounding rock is located at the position of the coal pillar. The maximum stress on the top of the gasifier cavities decreases with the increase in the width of the coal pillar, and the decreasing trend gradually reduces when the coal pillar width is approximately 11 m. As the coal pillar width increases, the maximum stress on the coal pillar first increases and then slowly decreases. The maximum stress occurs at a coal pillar width of approximately 11 m. The maximum vertical stress at the roof of the drop-shaped gasifier cavities and the maximum vertical stress variation curve of the coal pillar for different coal pillar widths are shown in Figure 10(d).

The displacement field distribution of the surrounding rock in two adjacent gasifier cavities with different shapes and coal pillar widths at room temperature was obtained through simulations. The displacement field distribution of the surrounding rock in traditional rectangular gasifier cavities is shown in Figure 10(e). The maximum displacement of the roof plate initially decreases and then increases with the increase in the width of the coal pillar, primarily owing to the gradual increase in the stability of the coal pillar. When the width of the coal pillar is approximately 19–21 m, the sinkage of the roof plate is minimum. The maximum displacement of the coal pillar first decreases with the increase in the width of the coal pillar and then gradually becomes constant. When the width of the coal pillar is approximately 18–20 m, the maximum vertical displacement becomes constant. The maximum vertical displacement of the traditional rectangular gasifier cavities and the maximum vertical displacement variation curve of the coal pillar considering different coal pillar widths are shown in Figure 10(f). The displacement field distribution of the surrounding rock in drop-shaped gasifier cavities is shown in Figure 10(g). The maximum displacement of the direct roof decreases with the increase in the coal pillar width, primarily owing to the increase in the stability of the coal pillar. When the width of the coal pillar is approximately 12 m, the decreasing trend of the maximum displacement of the roof slab gradually reduces. The maximum displacement of the coal pillar decreases with the increase in the coal pillar width. This decreasing trend gradually reduces when the width of the coal pillar is approximately 12 m. The vertical displacement graph of the maximum vertical displacement of the roof of the drop-shaped gasifier cavities and the maximum vertical displacement of the coal pillar for different coal pillar widths at room temperature are shown in Figure 10(h).

Comparing the stress field and displacement field distributions of the two gasifier cavity shapes at room temperature, the vertical stress in the surrounding rock of the traditional rectangular gasifier cavities is higher than that in the surrounding rock of the drop-shaped gasifier cavities. The stress influence range in the traditional rectangular gasifier cavities is wider than that in the drop-shaped gasifier cavities. The direct top/bottom in the traditional rectangular gasifier cavities present tensile stress states, and the rock around the drop-shaped gasifier cavities presents typical compressive stress states. Owing to the intractability of the

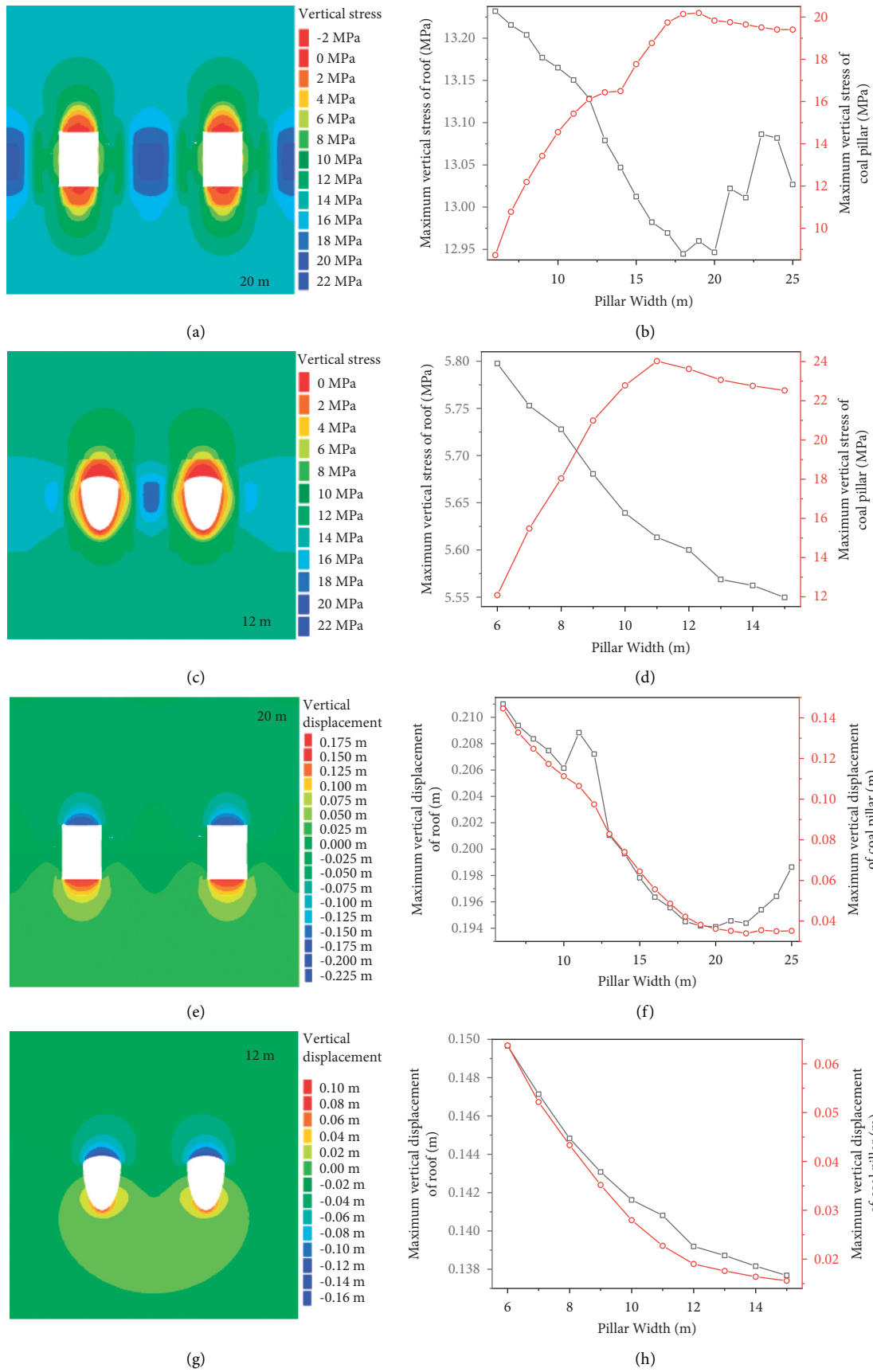

FIGURE 10: Simulation graph and maximum vertical stress/displacement variation curve considering different gasifier cavity shapes at room temperature.

rock, there are no obvious tensile stress areas, and the plastic area in the drop-shaped gasifier cavities is smaller than that in the traditional rectangular gasifier cavities. The displacement of the surrounding rock in the traditional rectangular gasifier cavities is higher than that in the drop-shaped gasifier cavities. Similarly, the vertical displacement of the coal pillar in the traditional rectangular gasifier cavities is higher than that in the drop-shaped gasifier cavities.

6. Influence of High Temperatures (700–1300°C) on the Surrounding Rock of Drop-Shaped Gasifier Cavities

6.1. Comparison of the Plastic Failure Area and Analysis of Reasonable Coal Pillar Width. The distribution of the plastic failure areas of the surrounding rock in two adjacent drop-shaped gasifier cavities with different coal pillar widths at high temperatures (700–1300°C) was obtained through simulations. As the temperature increased, the plastic area in the surrounding rock of the gasifier cavities gradually increased. The effect of different coal pillar widths on the distribution of plastic failure areas in adjacent drop-shaped gasifier cavities at 700°C is shown in Figure 11(a). When the width of the coal pillar is less than 16 m, it exhibits plastic failure; when the width of the coal pillar exceeds 16 m, a stable elastic area appears in the middle of the coal pillar. Shear failure primarily occurs in the surrounding rock, and the volume of the shear failure unit initially decreases rapidly and then decreases slowly with the increase in the coal pillar width; the decreasing trend reduces when the coal pillar width is approximately 17 m. The volume of the tensile failure unit initially decreases rapidly and then decreases slowly with the increase in the coal pillar width; the decreasing trend reduces when the coal pillar width is approximately 17 m. The ratio of the shear unit volume to the tensile unit volume decreases with the increase in the coal pillar width. The ratio of the shear unit volume to the tensile unit volume initially decreases rapidly and then decreases gradually with the increase in the coal pillar width, and the decreasing trend reduces when the coal pillar width is approximately 17 m. The volume change curves of different plastic failure methods with different pillar widths at 700°C are shown in Figure 12(a)–12(c). Therefore, the reasonable coal pillar width between two adjacent drop-shaped gasifier cavities at 700°C should not be less than 17 m.

Similarly, the distributions of the plastic failure areas and the volume change curves of adjacent drop-shaped gasifier cavities with different coal pillar widths and plastic failure methods at various elevated temperatures (850–1300°C) are shown in Figure 11(b) and 11(e) and Figure 12(a)–12(f), respectively. As the temperature increases, the shear failure volume and tensile failure volume units exhibit an exponential growth trend, and the ratio of the cut unit volume to the tensile unit volume exhibits an exponential decreasing trend. Therefore, at high temperatures, the reasonable coal pillar widths between two adjacent drop-shaped gasifier cavities should be at least 17 m (850°C), 18 m (1000°C), 19 m (1150°C) and 20 m (1300°C).

The distribution of the plastic failure areas of the surrounding rock in two adjacent drop-shaped gasifier cavities with reasonable coal pillar widths at high temperatures (700–1300°C) is shown in Figure 12(g). The failure volume of the surrounding rock of the gasifier cavities with reasonable coal pillar widths increases with the increase in temperature, and the surrounding rock primarily experiences shear failure. The failure range of the surrounding rock changes linearly, and the volume under different failure methods also increases approximately linearly with the increase in temperature. Additionally, the shear failure volume increases at a rate of 7.35 m^3/°C with the increase in temperature; the tension failure volume increases at a rate of 0.21 m^3/°C with the increase in temperature; and the overall failure area volume increases at a rate of 7.56 m^3/°C with the increase in temperature. In contrast, the ratio of the shear unit volume to the tension unit volume decreases linearly with the increase in temperature, at a rate of 0.04°C^{-1}.

6.2. Comparative Analysis of Stress Field and Displacement Field. The stress fields of the surrounding rocks in two adjacent drop-shaped gasifier cavities with different coal pillar widths at high temperatures (700–1300°C) was obtained through simulations. The distribution of the stress field of the surrounding rocks in two adjacent drop-shaped gasifier cavities with different coal pillar widths at 700°C is shown in Figure 13(a). The maximum stress on the coal pillar occurs at the centre of the coal pillar. The maximum stress initially increases and then gradually decreases as the width of the coal pillar increases, and the maximum stress reaches the peak value when the coal pillar width is approximately 15–16 m. The maximum stress on the top plate of the gasifier cavities decreases as the width of the coal pillar increases, and the decreasing trend reduces when the width of the coal pillar is approximately 16 m. The maximum vertical stress variation curves at the tops of the drop-shaped gasifier cavities at different temperatures and pillar widths and the maximum vertical stress variation curve at the pillar of the drop-shaped gasifier cavities at different temperatures and pillar widths are shown in Figure 13(b) and 13(c).

The maximum vertical stresses on the direct top of the two adjacent drop-shaped gasifier cavities and the coal pillar, considering a reasonable coal pillar width at high temperatures, are shown in Figure 13(d). As the temperature increases, the vertical stress on both the direct top and coal pillar decrease exponentially; the maximum vertical stress on the direct top gradually decreases with the increase in temperature, whereas the decrease in the maximum vertical stress on the coal pillar reduces with the increase in temperature. Therefore, the high-temperature failure of the rock decreases the bearing capacity of the rock and increases the plastic area around the gasifier cavities, thereby decreasing the peak stress on the surrounding rock in the gasifier cavities.

The displacement field of the surrounding rock in the two adjacent drop-shaped gasifier cavities with different coal pillar widths at high temperatures (700–1300°C) was obtained through simulations. The displacement field

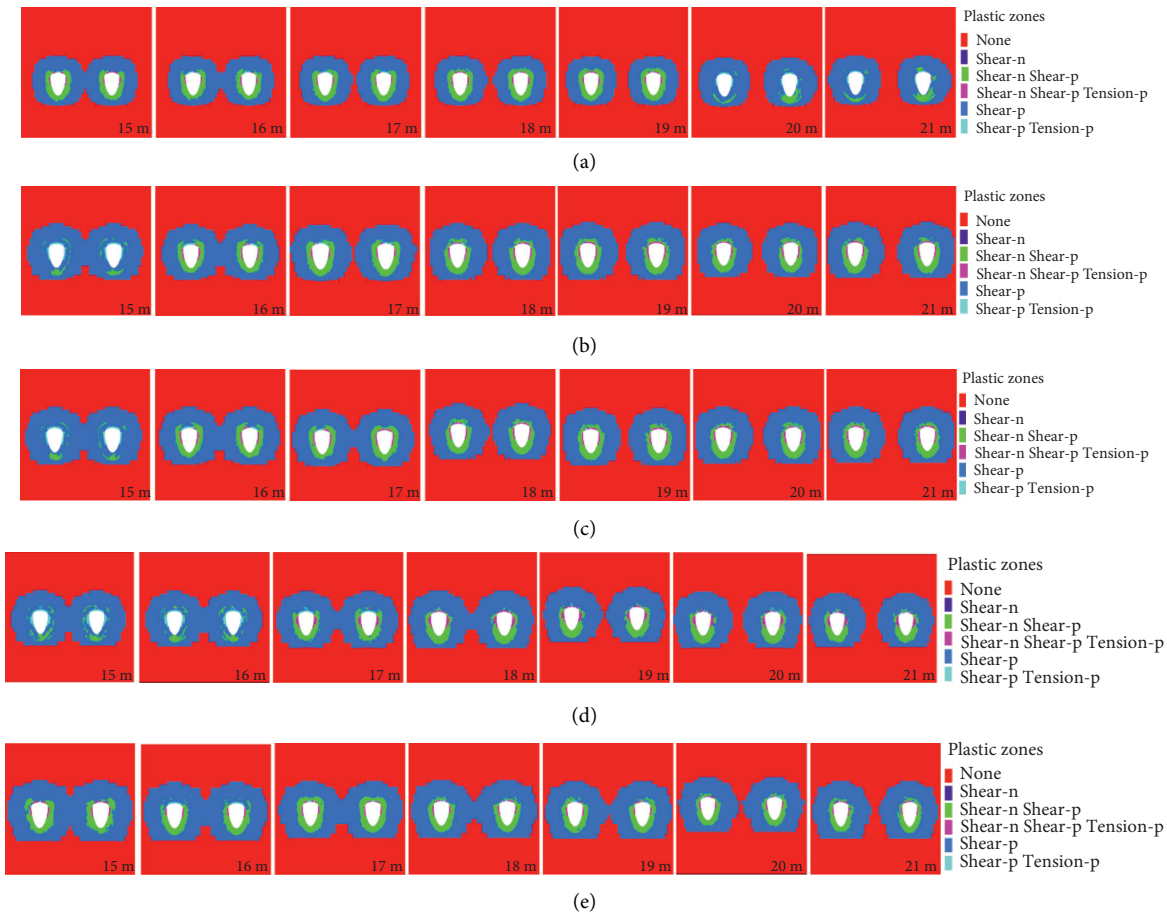

Figure 11: Plastic failure areas of the drop-shaped gasifier cavities for different coal pillar widths under different high-temperatures: (a) 700 ˚C; (b) 850 ˚C; (c) 1000 ˚C; (d) 1150 ˚C; (e) 1300 ˚C.

distribution of the surrounding rock in the two adjacent drop-shaped gasifier cavities with different coal pillar widths at 700˚C is shown in Figure 13(e). The maximum displacement of the coal pillar decreases with the increase in the coal pillar width, and the decreasing trend reduces considerably when the coal pillar width is approximately 16 m. The maximum displacement of the top plate of the gasifier cavities decreases with the increase in the coal pillar width, primarily because the stability of the coal pillar increases. The decreasing trend of the maximum sinking of the top plate reduces when the coal pillar width is approximately 16 m. The variation curve of the maximum vertical displacement of the roof of the drop-shaped gasifier cavities at different temperatures and with different coal pillar widths, and the variation curve of the maximum vertical displacement of the coal pillar of the drop-shaped gasifier cavities at different temperatures and with different coal pillar widths are shown in Figure 13(f) and 13(g).

The displacement distribution of the surrounding rock of the two adjacent drop-shaped gasifier cavities at a high temperature, the maximum vertical displacement of the roof of the drop-shaped gasifier cavities at different temperatures, and the variation curve of the maximum vertical displacement of the coal pillar with reasonable coal pillar widths are shown in Figure 13(g). The maximum vertical displacement on the direct top of the two adjacent drop-shaped gasifier cavities and the coal pillar, considering a reasonable coal pillar width at high temperatures, are shown in Figure 13(h). As the temperature increases, the vertical displacement increases; specifically, the vertical displacement of the coal pillar experiences an exponential increase. This can be attributed to the high-temperature failure of the rock. Under the same conditions, as the temperature increases, the plastic area around the gasifier cavities increases and the bearing capacity of the surrounding rock decreases. Consequently, the displacement increases.

Combining these results with those obtained at room temperature, and comparing the stress field and plastic area for the two forms of gasifier cavities, it can be inferred that drop-shaped gasifier cavities suppress the settlement of the direct top and the expansion of the plastic area of the central coal pillar. Furthermore, the high-temperature failure of the surrounding rock in the gasifier cavities increases the stress field and plastic area. In summary, a reasonable coal pillar width for traditional rectangular gasifier cavities is 21 m, whereas that for drop-shaped gasifier cavities at room temperature, 700˚C, 850˚C, 1000˚C, 1150˚C, and 1300˚C, is 12 m, 17 m, 17 m, 18 m, 19 m, and 20 m, respectively. Therefore, the reasonable coal pillar width of drop-shaped gasifier cavities at room temperature < the reasonable coal pillar width of drop-shaped gasifier cavities at high

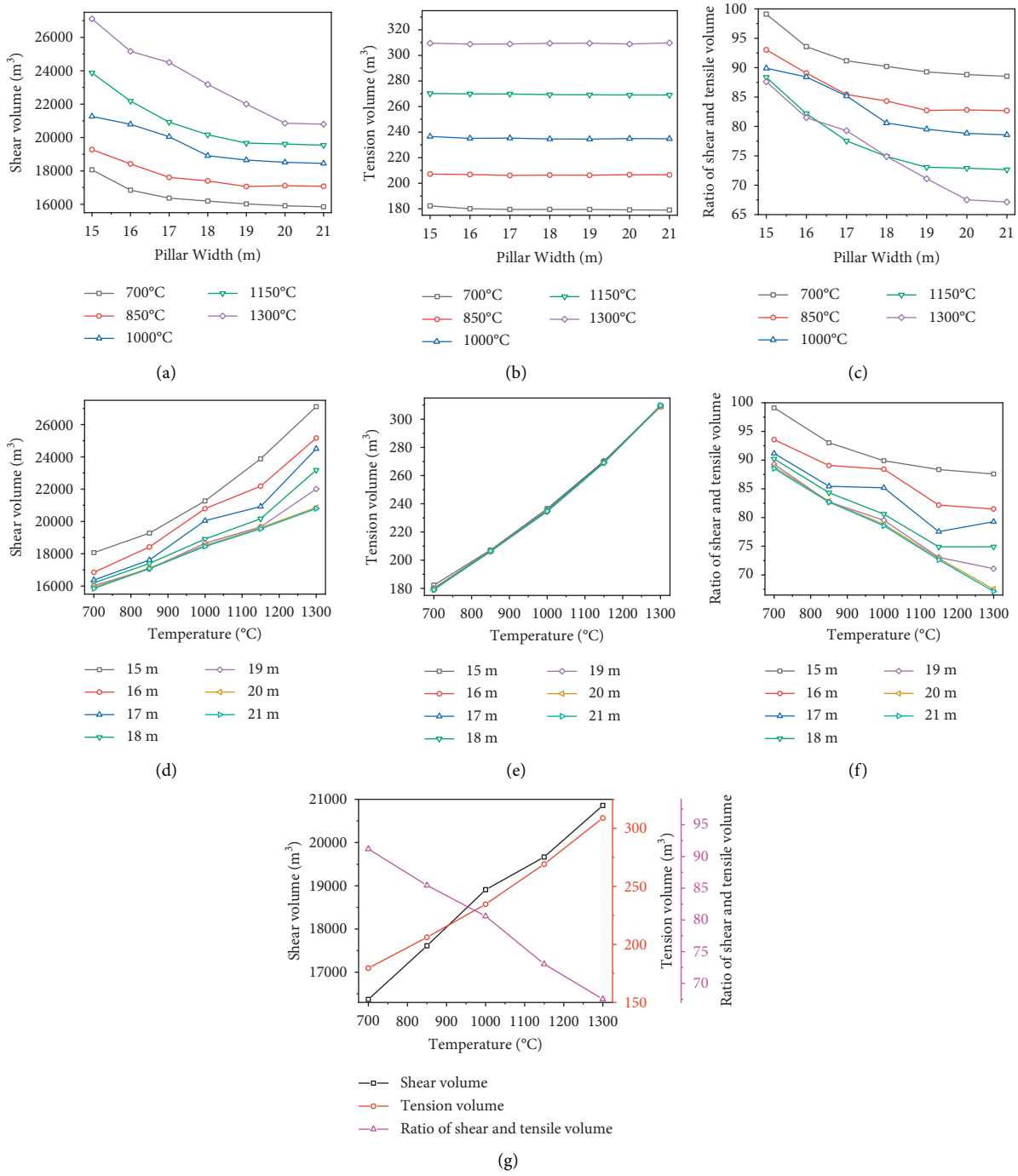

Figure 12: The volume change curves of the drop-shaped gasifier cavities at high temperature with different plastic failure methods for different pillar widths.

temperatures < the reasonable coal pillar width of traditional rectangular gasifier cavities. This implies that the results of numerical simulations that use traditional rectangular gasifier cavities instead of drop-shaped gasifier cavities will exceed the actual values for drop-shaped gasifier cavities.

6.3. Relationship between Coal Pillar Width and Temperature at High Temperatures (700–1300°C). The distribution of the stress field and plastic failure areas of the surrounding rock in two adjacent drop-shaped gasifier cavities with reasonable coal pillar widths at different temperatures (700–1300°C) was derived as shown in Figure 14 and Table 3. As the temperature increases, the range of the rock failure temperature increases, and the degree of attenuation of the physical parameters of the surrounding rock increases further, which increases the influence range of the gasifier cavities. Furthermore, the range and degree of superposition of the vertical stress of the gasifier cavities on the coal pillar becomes elevated, and the reasonable coal pillar width must

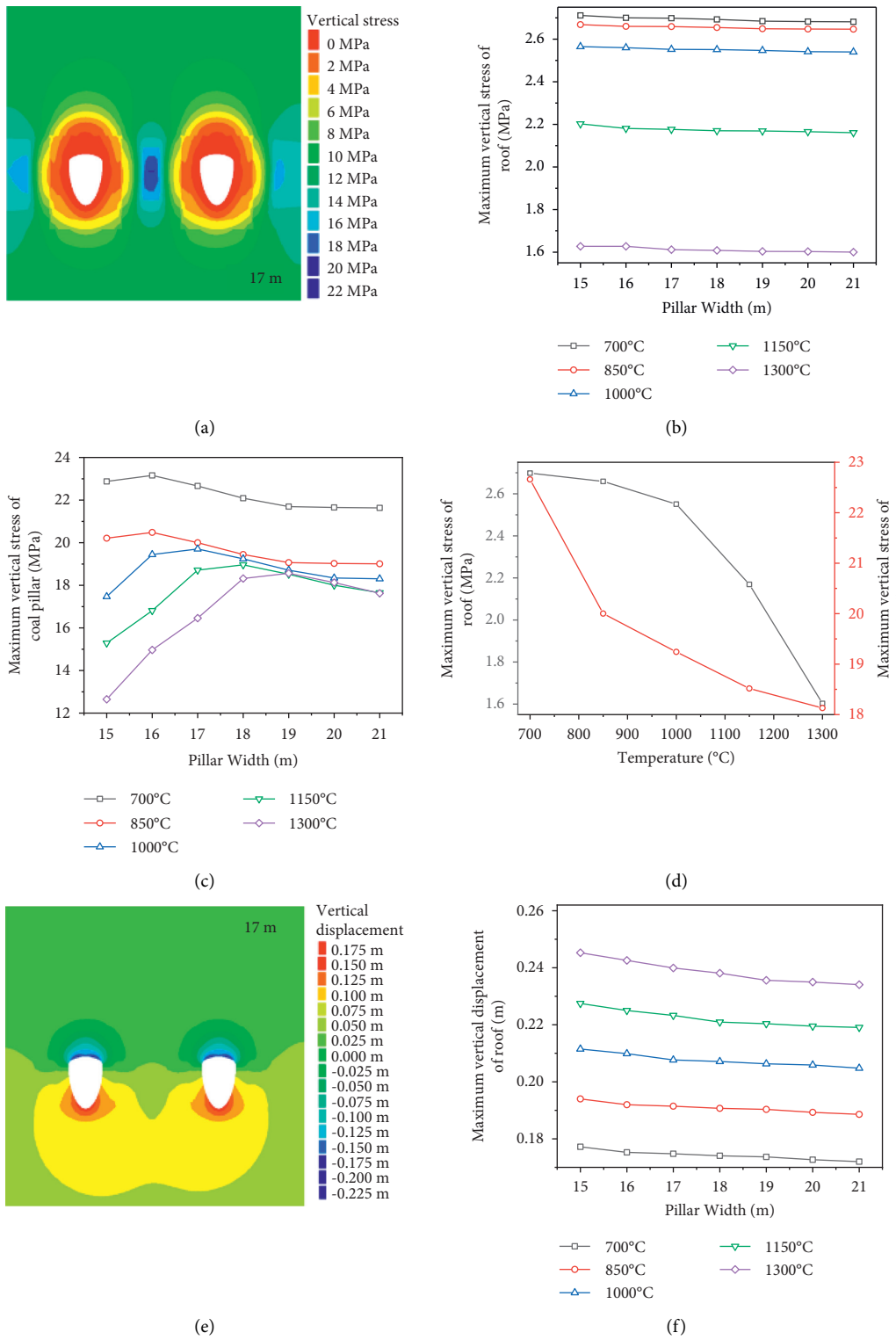

Figure 13: Continued.

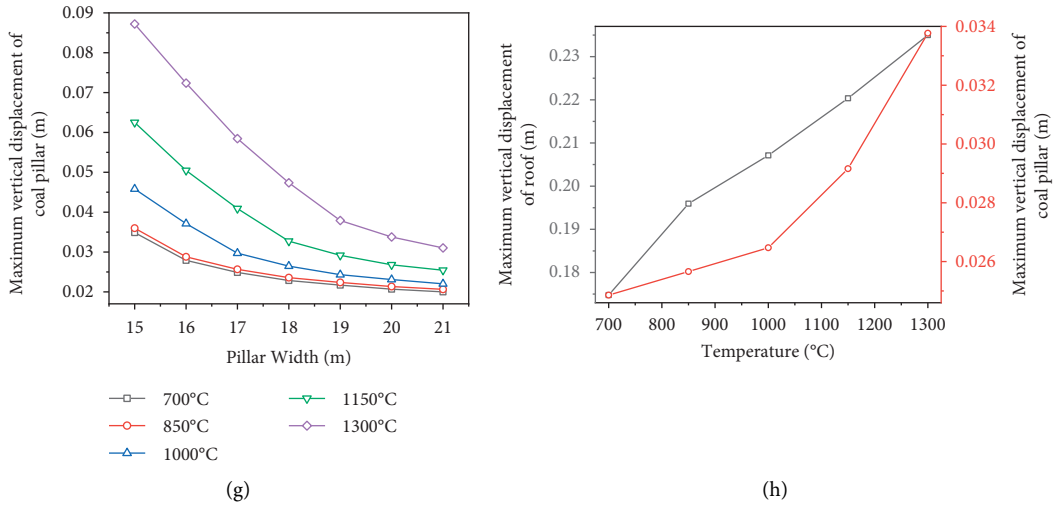

Figure 13: The volume change curves of the drop-shaped gasifier cavities at high temperature with different plastic failure methods for different pillar widths.

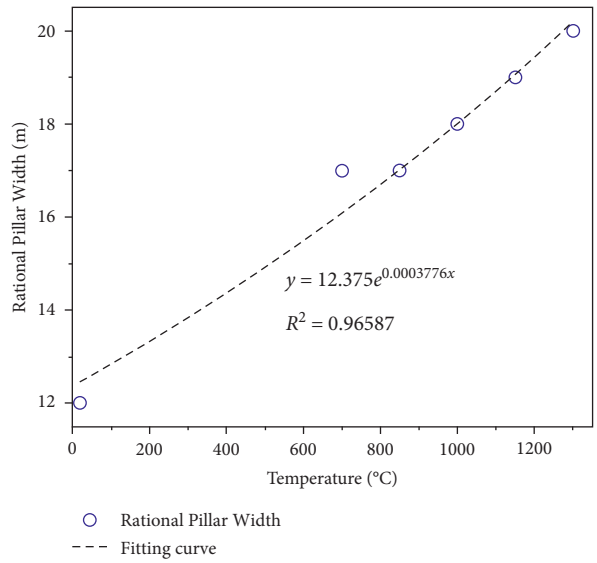

Figure 14: The reasonable coal pillar width under different temperature (700 ˚C–1300 ˚C).

Table 3: The reasonable coal pillar widths between two adjacent drop-shaped gasifier cavities at different temperatures.

Temperatures	20 ˚C (m)	700 ˚C (m)	850 ˚C (m)	1000 ˚C (m)	1150 ˚C (m)	1300 ˚C (m)
The reasonable coal pillar widths	12	17	17	18	19	20

increase accordingly. The increase in temperature is consistent with the plastic failure areas. The variation law of the reasonable coal pillar width with the rock temperature at different temperatures conforms to the exponential form, which indicates that the higher the rock temperature, the wider the reasonable coal pillar width.

7. Conclusions

(1) The surrounding rock in gasifier cavities is influenced by the high temperature associated with underground coal gasification, and the degree of influence gradually decreases with the increase in the distance from the gasifier cavity. The mechanical properties of surrounding rock at different temperatures (20–700˚C) were obtained experimentally. As the temperature increases, the relative density and relative tensile strength decrease approximately linearly, the relative modulus of elasticity decreases in the form of a power function, and the relative Poisson's ratio decreases exponentially.

(2) FLAC^{3D} was used to analyse the surrounding rock failure of drop-shaped gasifier cavities. In the numerical model, the mechanical parameters of the

surrounding rock were assigned a gradient distribution based on the temperature propagation law and the experimental results. The temperature of the surrounding rock has a significant influence on the stability of the coal pillar, and the surrounding rock primarily undergoes shear failure. As the temperature of the surrounding rock increases, the width of the stable coal pillar increases approximately exponentially; the reasonable widths of coal pillars between drop-shaped gasifier cavities are 12 m (room temperature), 17 m (700°C and 850°C), 18 m (1000°C), 19 m (1150°C), and 20 m (1300°C).

(3) The reasonable coal pillar widths of drop-shaped and traditional rectangular gasifier cavities were compared through numerical simulations. The reasonable coal pillar width of a traditional rectangular gasifier cavity at room temperature is approximately 21 m, which is significantly higher than that of a drop-shaped gasifier cavity (12 m). Therefore, the shape of the gasifier cavity has a significant influence on the stability of the coal pillar and should not be simplified to the traditional rectangular shape.[25, 26]

Data Availability

The data used to support the findings of this study are included within the article.

Conflicts of Interest

The authors declare that they have no conflicts of interest.

Acknowledgments

The authors would like to thank the Beijing Outstanding Young Scientist Program (BJJWZYJH01201911413037) are thankful for the projects (Grant Nos: 51622404 and 41877257) supported by NSFC of China.

References

[1] L. Yu, "Utilization of abandoned coal Resources to promote the development of underground coal gasification technology in China," *Coal Science and Technology*, vol. 41, no. 5, pp. 1–3, 2013, (In Chinese).

[2] H. Xie, F. Gao, Y. Ju et al., "Theoretical and technological conception of the fluidization mining for deep coal Resources," *Journal of China Coal Society*, vol. 3, pp. 547–556, 2017, (In Chinese).

[3] S. Wang, Q. Sun, J. Qiao, and S. Wang, "Geological guarantee of coal green mining," *Journal of China Coal Society*, vol. 1, pp. 8–15, 2020, (In Chinese).

[4] J. Zuo, Y. Sun, H. Liu et al., "Multi - scale failure mechanics of rock in mining engineering," *Journal of Mining Science and Technology*, vol. 6, no. 5, pp. 509–523, 2021.

[5] M. Najafi, S. M. E. Jalali, and R. Khalokakaie, "Thermal-mechanical-numerical analysis of stress distribution in the vicinity of underground coal gasification (UCG) panels," *International Journal of Coal Geology*, vol. 134-135, pp. 1–16, 2014.

[6] J. Wang, Z. Wang, L. Xin, Z. Xu, J. Gui, and X. Lu, "Temperature field distribution and parametric study in underground coal gasification stope," *International Journal of Thermal Sciences*, vol. 111, pp. 66–77, 2017.

[7] W.-g. Huang and Z.-t. Wang, "Mechanical performance evolution and size determination of strip coal pillars with an account of thermo-mechanical coupling in underground coal gasification," *International Journal of Rock Mechanics and Mining Sciences*, vol. 142, no. 4, 104755 pages, 2021.

[8] Y. Lu, L. Wang, F. Tang, and Y. He, "Fracture evolution of overlying strata over gasifier cavities under thermal-mechanical interaction during underground coal gasification," *Journal of China Coal Society*, vol. 8, pp. 1292–1298, 2012, (In Chinese).

[9] Q. Tan, "Numerical comparison analysis of thermal stress field of stratified rock in elastic or non-linear states at high temperature," *Mining Research and Development*, vol. 3, pp. 58–61, 2011, (In Chinese).

[10] Y. Derbin, J. Walker, D. Wanatowski, and A. Marshall, "Soviet experience of underground coal gasification focusing on surface subsidence," *Journal of Zhejiang University - Science*, vol. 16, no. 10, pp. 839–850, 2015.

[11] S. Daggupati, R. N. Mandapati, S. M. Mahajani et al., "Laboratory studies on combustion cavity growth in lignite coal blocks in the context of underground coal gasification," *Energy*, vol. 35, no. 6, pp. 2374–2386, 2010.

[12] F. Laouafa, R. Farret, S. Vidal-Gilbert, and J.-B. Kazmierczak, "Overview and modeling of mechanical and thermo-mechanical impact of underground coal gasification exploitation," *Mitigation and Adaptation Strategies for Global Change*, vol. 21, no. 4, pp. 547–576, 2016.

[13] L. Xin, Z. Wang, E. Huang, K. Zhao, Y. Ju, and S. He, "Measurement analysis of overlying strata movement and surface subsidence by UCG strip mining," *Journal of Mining & Safety Engineering*, vol. 31, no. 3, pp. 447–455, 2014, (In Chinese).

[14] H. Li, G. Guo, J. Zha, Y. He, Z. Wang, and S. Qin, "Stability evaluation method for hyperbolic coal pillars under the coupling effects of high temperature and ground stress," *Environmental Earth Sciences*, vol. 76, no. 20, p. 704, 2017.

[15] N. Zhao, E. B. Du, M. Li, J. X. Zhang, and C. W. Dong, "Determination of the stability of residual pillars in a room-and-pillar mining goaf under eccentric load," *Energy Reports*, vol. 7, pp. 9122–9132, 2021.

[16] P. Le Quang, V. Zubov, and T. P. Duc, "Design a reasonable width of coal pillar using a numerical model. A case study of khe cham basin," *Web of Conferences*, vol. 174, Article ID 01043, 2020.

[17] T.-b. Zhao, M.-l. Xing, W.-y. Guo, C.-w. Wang, and B. Wang, "Anchoring effect and energy-absorbing support mechanism of large deformation bolt," *Journal of Central South University*, vol. 28, no. 2, pp. 572–581, 2021.

[18] Y. Tan, W. Guo, Y. Tan, T. Zhao, Y. Xiao, and Y. Chen, "Energy release law of roadway surrounding rock and energy-driven rock burst mechanism," *Journal of China Coal Society*, 2021, (In Chinese).

[19] J. Zuo, H. Liu, D. Liu, J. Wang, T. Zhang, and F. Xu, "Study on large deformation mechanism and concrete-filled steel tubular support technology for ventilation shaft roadway," *Bulletin of Engineering Geology and the Environment*, vol. 80, no. 8, pp. 6245–6262, 2021.

[20] G. Wu, W. Yu, J. Zuo, and S. Du, "Experimental and theoretical investigation on mechanisms performance of the rock-coal-bolt (RCB) composite system," *International Journal of*

Mining Science and Technology, vol. 30, no. 6, pp. 759–768, 2020.

[21] M. Yu, J. Zuo, Y. Sun, C. Mi, and Z. Li, "Investigation on fracture models and ground pressure distribution of thick hard rock strata including weak interlayer," *International Journal of Mining Science and Technology*, 2021.

[22] J. Zuo, Y. Shi, D. Liu, Y. Sun, and Y. Chen, "The equivalent ellipse model and simulation analysis of Destressing by Cutting Groove in deep soft rock roadway," *Journal of China University of Mining & Technology*, vol. 48, no. 1, pp. 1–11, 2019.

[23] B. Lei, H. Li, J. Zuo, H. Liu, M. Yu, and G. Wu, "Meso-fracture mechanism of Longmaxi shale with different crack-depth ratios: experimental and numerical investigations," *Engineering Fracture Mechanics*, vol. 257, Article ID 108025, 2021.

[24] J. Xi, Z. Wang, K. Liang, X. Bian, and H. Zhu, "Reserch status and development trend of model experiment for underground coal gasification," *Coal Science and Technology*, vol. 4, pp. 131–136+99, 2015, (In Chinese).

[25] J. Zuo, X. Wei, Y. Shi, C. Liu, M. Li, and R. Wong, "Experimental study of the ultrasonic and mechanical properties of a naturally fractured limestone," *International Journal of Rock Mechanics and Mining Sciences*, vol. 125, pp. 1–12, 2020.

[26] H. Song, J. Zuo, H. Liu, and S. Zuo, "The strength characteristics and progressive failure mechanism of soft rock-coal combination samples with consideration given to interface effects," *International Journal of Rock Mechanics and Mining Sciences*, vol. 138, 2021.

[27] Z. Li, J. Zuo, Y. Shi, F. Xu, M. Yu, and C. Mi, "An experimental study on the slippage effects of sandstone under confining pressure and low pore pressure conditions," *Geofluids*, vol. 2020, pp. 1–17, 2020.

[28] M. Zhao, D. Dong, G. Lin, G. Wang, and K. Li, "Evolution laws of temperature field and fracture field in UCG," *Coal Technology*, vol. 6, pp. 177–179, 2016, (In Chinese).

[29] H. Akbarzadeh and R. J. Chalaturnyk, "Structural changes in coal at elevated temperature pertinent to underground coal gasification: a review," *International Journal of Coal Geology*, vol. 131, pp. 126–146, 2014.

[30] M. Zhao, D. Dong, and K. Tian, "Change mechanism simulation study of the overlying strata temperature field and fracture field in UCG," *Journal of Mining Science and Technology*, vol. 2, no. 1, pp. 1–6, 2017, (In Chinese).